THE JOURNAL OF PHYSICAL CHEMISTRY C

Article

Cite This: J. Phys. Chem. C 2019, 123, 16146−16152

pubs.acs.org/JPCC

Insight on the Sequential Vapor Infiltration Mechanisms of Trimethylaluminum with Poly(methyl methacrylate), Poly(vinylpyrrolidone), and Poly(acrylic acid)

Grant T. Hill, Dennis T. Lee, Philip S. Williams, Craig D. Needham, Erinn C. Dandley, Christopher J. Oldham, and Gregory N. Parsons*

Department of Chemical and Biomolecular Engineering, North Carolina State University, 911 Partners Way, Raleigh, North Carolina 27695, United States

ABSTRACT: The sequential vapor infiltration (SVI) method, based on atomic layer deposition chemistry, allows the creation of a polymer−inorganic hybrid material through the diffusion of metal−organic vapor reagents into a polymer substrate. This study investigates the reactivity of the ester, amide, and carboxylic acid functional groups of poly(methyl methacrylate) (PMMA), poly(vinylpyrrolidone) (PVP), and poly(acrylic acid) (PAA), respectively, in the presence of trimethylaluminum (TMA) vapor. This work explores the possible reaction mechanisms of these functional groups through in situ Fourier transform infrared spectroscopy and ab initio quantum chemical analysis. At temperatures of ≤100 °C, TMA physisorbs to the carbonyl groups of PMMA. As the temperature is increased, TMA forms a covalent bond with PMMA. TMA physisorbs to PVP and then partially desorbs in the presence of water for all studied temperatures of ≤150 °C. PAA readily reacts with TMA to form a covalent bond with the carbonyl group at 60 °C. This increased reactivity is attributed to the acidic proton in the carboxylic acid moiety based on TMA's reactivity with hydroxyl-terminated surfaces and ab initio calculations. At temperatures of ≥100 °C, TMA catalyzes anhydride formation in PAA. These insights will help with the prediction of chemical interactions in SVI processes for the development of organic−inorganic hybrid materials.

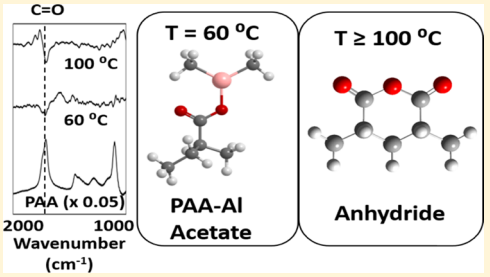

INTRODUCTION

Different subclasses of vapor-phase infiltration (VPI) have been active areas of research for modifying polymers to produce polymer−inorganic hybrid materials.[1−4] The subclasses, multiple pulse infiltration, sequential infiltration synthesis, and sequential vapor infiltration, are differentiated by their precursor-dosing sequences. VPI originates from atomic layer deposition (ALD), which is a vapor-phase thin-film deposition technique. ALD has been actively utilized to impart effective nucleation sites onto diverse polymeric fibrous scaffolds, such as poly(acrylic acid), poly(ethylene terephthalate), or nylon-6.[3,4] Therefore, highly porous and functional materials of metal−organic frameworks (MOFs), for instance, can be uniformly coated onto ALD-treated surfaces, thus becoming MOF/fabric composite materials functioning as promising catalysts.[5−10]

Although VPI is based on the same sequential self-limiting chemistry as ALD, it utilizes the vapor-phase precursor's diffusion and reaction in the polymer bulk. The VPI processing scheme is as follows: precursor absorption into the polymer, precursor diffusion within the polymer bulk, and entrapment of precursor within the polymer.[1] This process changes the bulk structure and functionality of the polymer and leads to the formation of new, hybrid materials, which have unique properties. Some of these previously studied polymer−inorganic hybrid materials have improved mechanical properties, improved nanopatterning, improved imaging, increased conductivity, and enhanced vapor-barrier properties.[11−18] To better understand these improvements, an understanding of the polymer−precursor reaction mechanism is necessary. This knowledge will support process design and property improvements for various applications. Insight into the reaction mechanism can also aid in understanding unexplored metal−organic/polymer combinations.

In this work, we use a subclass of VPI called sequential vapor infiltration (SVI) to study reaction mechanisms. Other VPI subclasses alternate between precursors A and B during the dosing sequence, whereas SVI starts with a dosing sequence of precursor A and then finishes with a dosing sequence of precursor B. The SVI process introduces and holds a vapor precursor, usually a metal−organic, in a closed, heated reactor environment with the polymeric substrate.[2,19,20] The extent of diffusion and reaction of the vapor precursors in the polymer bulk is dependent on the polymer bulk properties, the precursor exposure time, the reaction temperature, and the chemical interactions between polymer functional groups and the vapor precursor.[21,22] After the hold time, the reactor is purged of byproduct vapor with an inert gas, such as nitrogen. The vapor reactant exposure process is repeated as desired and then finished with a coreactant step, usually water.

Received: March 6, 2019
Revised: June 12, 2019
Published: June 14, 2019

DOI: 10.1021/acs.jpcc.9b02153
J. Phys. Chem. C 2019, 123, 16146−16152

One of the most studied SVI and ALD reactions is between trimethylaluminum (TMA) and poly(methyl methacrylate) (PMMA).[2,23−25] Biswas et al. found that PMMA goes through a two-step reaction in the presence of TMA. The first step is a fast, reversible reaction that produces a physisorbed complex. The second step is a slow, irreversible reaction of the physisorbed complex that produces a covalently bonded product structure. They proposed that the product formation breaks the PMMA carbonyl group to produce O−Al−$(CH_3)_2$ by a TMA methyl group shifting to the carbon center. The TMA that is trapped in the PMMA bulk will continue to slowly react to completion. They concluded that the product concentration is increased by shorter purge times and longer TMA exposure.[23] Dandley et al. compared in situ FTIR findings to calculated spectra of possible product structures. They determined that the second step of the reaction mechanism is a pericyclic reaction that yields a covalent bond of Al−$(CH_3)_2$ with the O originally in the carbonyl group. They found that the TMA methyl group does not shift to the carbon center but instead reacts with the PMMA methoxy group, thus producing an ester carbonyl and ethane vapor. They found that the second step of the reaction becomes more favorable as the temperature was increased from 110 to 150 °C for a 150 TMA dose SVI process, where each TMA dose has a 60 s TMA exposure and a 30 s purge. Higher temperatures make the second reaction step more favorable than the desorption of the complex formed in the first step.[2] In this study, we were able to confirm the TMA−PMMA product structure proposed by Dandley et al. with the spectral analysis.

TMA's small size and high reactivity make it suitable for the SVI process. Since TMA is a strong Lewis acid, these reactions usually begin with TMA forming a Lewis acid/base adduct with a strong Lewis base. PMMA is a good candidate for SVI because it has a large free volume and the carbonyl group is a strong Lewis base, which makes it favorable for the adduct formation with TMA. Once the first adduct is formed, the TMA−PMMA reactivity may be enhanced since TMA is also a strong Lewis acid catalyst.[26] Additionally, PMMA is not reactive enough to block TMA diffusion; polymers that have more reactive groups on the surface will prefer surface growth over infiltration.[27]

To further understand this and other mechanisms, this work explores the effects of polymer functional groups on TMA infiltration and reaction. Among those functional groups of interest are the side-chain amide, methyl ester, and carboxylic acid groups that are prominent in poly(vinylpyrrolidone) (PVP), PMMA, and poly(acrylic acid) (PAA), respectively. The functional group effects are studied with respect to the temperature dependence of the process. The reaction mechanisms are studied with in situ Fourier transform infrared spectroscopy (FTIR) and verified with ab initio quantum chemistry analysis. These results highlight chemical functionality as a critical factor in predicting temperature-dependent chemical interactions for vapor precursors infusing into a polymer. The presence of an acidic proton promotes covalent bond formation between the polymer and the metal−organic material. When an acidic proton is not present, the reactivity is related to the Lewis acid adduct stability.

METHODS

Poly(vinylpyrrolidone) (PVP, Fisher BioReagents, MW 40 000), poly(methyl methacrylate) (PMMA, Fluka Analytical, MW 97 000), poly(acrylic acid) (PAA, Aldrich Chemistry, MW 1800), and trimethylaluminum (TMA, Strem Chemicals, min. 98% pure) were used as received. The Si substrates were cleaned with acetone and dried by rotation at 2000 rpm for 1 min. The polymer solutions created were (i) 2.5 wt % of PVP in chloroform (Sigma-Aldrich), (ii) 5 wt % PMMA in toluene (Sigma-Aldrich), and (iii) 111.12 mg/mL of PAA in 1:1 ethanol (Sigma-Aldrich): deionized (DI) water. The PVP, PMMA, and PAA solutions were flooded onto the Si substrates and spun at 7380, 4140, and 3690 rpm, respectively, for 40 s to create 200 nm thin films. The polymer solution concentrations and rotation rates were previously optimized to form the desired thin-film thickness, which were characterized by spectroscopic ellipsometry (J.A. Woollam Co., Inc.) and by profilometry (Veeco Dektak 150). The remaining solvent was removed by heating the samples on a hot plate. PVP was heated for 1 min at 120 °C, PMMA was heated for 2 min at 200 °C, and PAA was heated for 3 min at 200 °C.

The samples were placed into a custom-made, viscous-flow, hot-walled vacuum reactor. The reactor was kept at about 800 mTorr and operated at temperatures between 60 and 150 °C. TMA was dosed into the reactor while closing all ports into and out of the reactor for a set time. High-purity nitrogen gas (Machine & Welding Supply Co.) that was further purified with an Entegris GateKeeper upstream of the reactor input was used to purge the reactor. This was repeated n times and then finished by a dose of DI water and a final purge. The water dosage was used to preclude the TMA-coated samples from reacting with atmospheric water. The typical dosing scheme was a 1 s TMA dose, a 60 s hold, and a 30 s purge. This was completed by a 1 s water dose and a 45 s purge. The scheme is denoted $[(1/60/30) \times n + (1/45)]$. For the remainder of this article, a "TMA dose" will refer to the listed scheme and will be reported as a number of TMA dose repeats (n).

Changes in chemical bonding were measured using an in situ Fourier transform infrared spectrophotometer incorporated into the reactor. The samples were preheated for 30 min in the reactor at 140 °C under vacuum while flowing N_2 gas to remove any volatile species from the polymer samples. The system was cooled to TMA infiltration temperature and equilibrated for 30 min for dosing sequences at 60, 100, and 150 °C. Spectra were taken after 10, 50, and 100 TMA doses and after the water dose. The reactor was purged for 2 min and then closed off after each set of TMA doses. Gates to the IR windows were then opened, and 200 spectra were obtained in the frequency range of 4000−400 cm^{-1} at a resolution of 4 cm^{-1}. An MCT-A detector was used through CsI IR windows.

Optimized geometries and frequencies of PMMA, PAA, PVP, TMA, PVP−TMA coordination complex, PMMA−TMA coordination complex, PMMA−Al acetate, PAA−acetate, and PAA−anhydride were calculated with Gaussian09.[28] The B3LYP density functional theory method was employed because of its ability to accurately predict frequency data.[29,30] All calculations were performed using a 6-31G++(d,p) basis set. We also used Gaussview to construct the model structures and view the calculated vibrations to verify modes in the experimental spectra.[31] Isopropylpyrrolidinone, methyl trimethylacetate, and 2-methylbutanoic acid were used as molecular models of PVP, PMMA, and PAA, respectively, due to their structural similarity to a single repeat unit of their respective polymers.

DOI: 10.1021/acs.jpcc.9b02153
J. Phys. Chem. C 2019, 123, 16146−16152

RESULTS AND DISCUSSION

Poly(methyl methacrylate). The mechanism for the reaction between TMA and PMMA during SVI processes at various temperatures has been explored previously.[2,23−25] In particular, the work by Dandley et al. found that at temperatures of ≥110 °C, a pericyclic reaction takes place, where the PMMA methoxy group reacts with a TMA molecule stabilized by the carbonyl coordination.[2] This current work on the PMMA−TMA reaction was done to verify the mechanism for our temperature set and to use this as a basis for comparison of the PMMA methyl ester to the amide moiety of the PVP and the carboxylic acid of the PAA during SVI processes with TMA. Figure 1 shows the FTIR spectra for

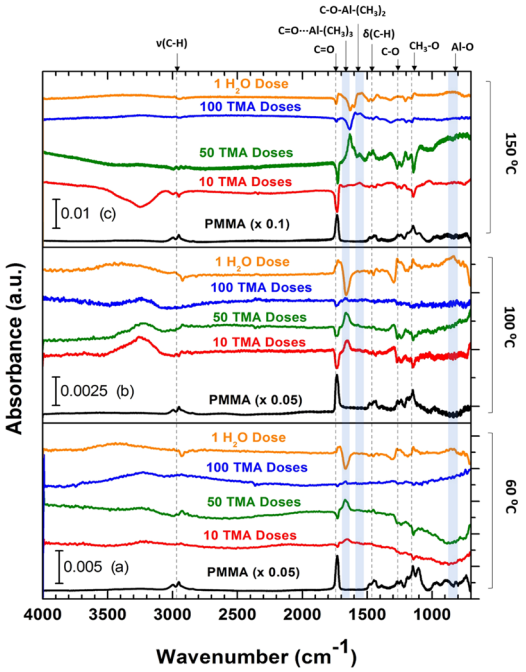

Figure 1. In situ FTIR spectra taken after *n* TMA doses at (a) 60 °C, (b) 100 °C, and (c) 150 °C on PMMA film. The black spectrum is the PMMA referenced to the bare silicon substrate, and all other spectra are referenced to the previous spectrum.

PMMA for the starting polymer, 10 TMA dose, 50 TMA dose, 100 TMA dose, and water dose at 60, 100, and 150 °C. The FTIR spectra are differential; for each temperature group, a spectrum references the spectrum below. The dotted lines mark the key modes found in the starting PMMA, and the blue bars mark modes that form due to the TMA.

For the starting PMMA polymer in Figure 1, the spectra showed peaks at 2950, 1732, 1448, 1265, and 1145 cm^{-1}, which correspond to C−H stretching (ν(C−H)), C═O stretching, C−H bending (δ(C−H)), C−O stretching, and CH_3−O stretching modes, respectively. The starting polymer spectrum is scaled for easier comparison to the TMA dose spectra. After the first 10 TMA doses at 60 and 100 °C (Figure 1a,b), both a negative-going mode at 1732 cm^{-1} and a positive-going mode at 1672 cm^{-1} are observed. This new peak at 1672 cm^{-1} corresponds to the lowered frequency of C═O stretching caused by the C═O···Al−$(CH_3)_3$ coordination bond. There are also positive-going modes at 2950 and 1448 cm^{-1} due to the increased presence of methyl groups from the TMA. There are negative-going modes at 1265 and 1145 cm^{-1} together with positive-going modes at 1195 and 1300 cm^{-1}, which indicate that the TMA−PMMA complex shifts the C−O and CH_3−O stretching frequencies. This trend continues for the next dosage steps with the step from 10 to 50 TMA doses resulting in the largest change. After the water dose, many of the changes from the TMA doses are reversed. The formation of the broad, positive-going mode at 820 cm^{-1} indicates Al−O cluster formation. This reversal indicates that at 60 and 100 °C, the TMA−PMMA complex is a metastable intermediate.

In Figure 1c, the 150 °C 10 TMA dose spectrum contains a positive-going mode at 1633 cm^{-1}, which corresponds to the TMA−PMMA complex. There is also the formation of a positive-going mode at 1562 cm^{-1}, which does not appear in lower-temperature PMMA spectra. The new mode at 1562 cm^{-1} continues to increase with following doses. The 100 TMA dose spectrum shows a negative-going mode at 1633 cm^{-1} and a positive-going mode at 1562 cm^{-1}, which indicate a transition of the metastable intermediate into a new formation. At this heightened temperature, the reactions involved proceed at a much higher rate, causing more products to be formed than at the lower temperatures. This accounts for the increased intensity of the signal seen in Figure 1c compared to that in Figure 1a,1b.

After the water dose, the 1562 cm^{-1} mode remains constant and the 1633 cm^{-1} mode is negative. The 1265 cm^{-1} and 1145 cm^{-1} modes of the water-dose spectrum remained constant, which is consistent with the corresponding C−O and CH_3−O stretching frequencies retaining the same modifications from the TMA doses. This evidence supports that at 150 °C, the PMMA and TMA form a covalently bonded product. The positive-going mode at 1562 cm^{-1} is the stretching of the new C═O bond, which is lower in frequency due to the new TMA−PMMA covalent bond. Therefore, the water dose did not break the covalent bond and it removed the remaining metastable TMA−PMMA complex intermediate, which is represented by the negative-going mode 1633 cm^{-1}. These experimentally observed findings are consistent with the work of Dandley et al.[2]

The proposed mechanism, shown in Figure 2a, is a pericyclic reaction where TMA coordination enables a methyl shift to form a C−C bond.[32] Frequencies were calculated using Gaussian09 for both the products of the metastable TMA−PMMA complex formed by the Lewis acid/base adduct and the PMMA−Al acetate formed by the temperature-activated pericyclic reaction.[28] Figure 2b shows the computed frequencies of the PMMA spectrum and the spectra differences of both the PMMA−TMA complex and the PMMA−Al acetate with PMMA. The represented structures of each spectrum are shown directly to the right in Figure 2c. These computed frequencies support the above mechanism for the PMMA−TMA complex and the aluminum acetate formation. The vibrational mode at 1732 cm^{-1} corresponding to the PMMA−TMA complex shifted to 1672 cm^{-1} matches the experimental data. The formation of the 1562 cm^{-1} peak at higher temperatures also matches the PMMA−Al acetate model. These results verify the temperature-activated covalent interaction that was explored by Dandley et al.[2]

Poly(vinylpyrrolidone). To further understand the effects of functional groups on the SVI process, the amide functional group found in PVP was studied due to the presence of the carbonyl group also found in the methyl ester in PMMA. Figure 3 shows the differential spectra for each set of TMA doses at 150 °C. Similar results were seen for all temperatures

DOI: 10.1021/acs.jpcc.9b02153
J. Phys. Chem. C 2019, 123, 16146−16152

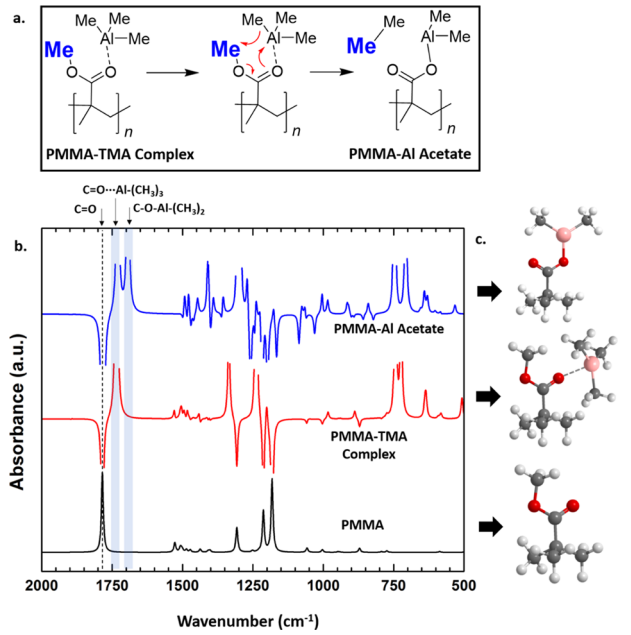

Figure 2. (a) Proposed pericyclic activation of ester to form metal acetate. (b) Computed vibrational spectra referenced to spectra calculated from PMMA structures in the absence of TMA. (c) Relaxed chemical structures calculated using ab initio analysis.

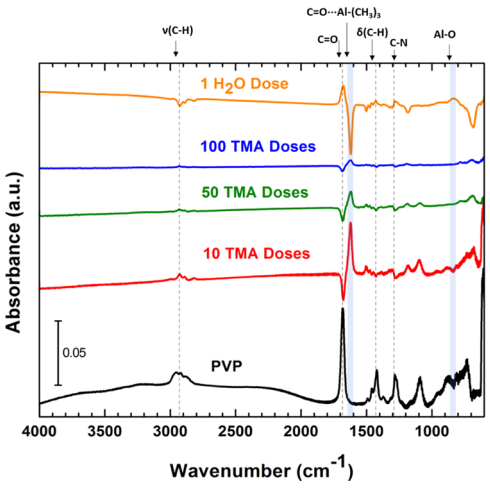

Figure 3. In situ FTIR spectra taken after *n* TMA doses at 150 °C on PVP film. The black spectrum is the PVP referenced to the bare silicon substrate, and all other spectra are referenced to the previous spectrum.

examined (60, 100, and 150 °C). Starting with the original PVP spectrum, the intense peak at 1680 cm^{-1} is the carbonyl stretching of the amide group (C═O). The positive-going modes at 2950 and 1420 cm^{-1} are related to C−H stretching (ν(C−H)) and C−H bending (δ(C−H)), respectively. The positive-going mode at 1280 cm^{-1} is the cyclic amide. After the first 10 TMA doses, there is a negative-going mode at 1680 cm^{-1} and a positive-going mode at 1621 cm^{-1}, which indicates the formation of the PVP−TMA complex. The C═O bond vibrations at 1680 cm^{-1} are changing due to the C═O···Al−$(CH_3)_3$ Lewis acid/base adduct formation, similar to the TMA−PMMA complex formation. The positive-mode formation after 10 TMA doses at 2950 cm^{-1} also indicates the increase in C−H bonding from the addition of TMA. The additional TMA doses shown by the 50 dose and 100 dose spectra display the same changes as the 10 dose spectrum except at lower intensities. The lower-intensity changes show that most of the TMA−PVP complex formation occurs within the first 10 TMA doses.

After one water dose, the positive- and negative-going modes are partially reversed. The negative-going 1621 cm^{-1} peak and positive-going 1680 cm^{-1} peak show the return of the original carbonyl-group-bonding structure (C═O). The water reacts with TMA that infiltrates into the polymer during the SVI processes leading to the formation of Al−O in the bulk, consistent with the broad positive-going mode at 820 cm^{-1}. This phenomenon was also observed in the PMMA. The reversal of the TMA−PVP complex from the water dose is consistent with C═O···Al−$(CH_3)_3$ being a metastable intermediate.

From the experimentally observed shift of the C═O-bonding mode from 1680 to 1621 cm^{-1} and its reversal from the water dose, we believe that TMA forms a complex with the PVP carbonyl moiety (PVP−TMA complex), as shown in Figure 4a. In Figure 4b, the spectra from ab initio frequency

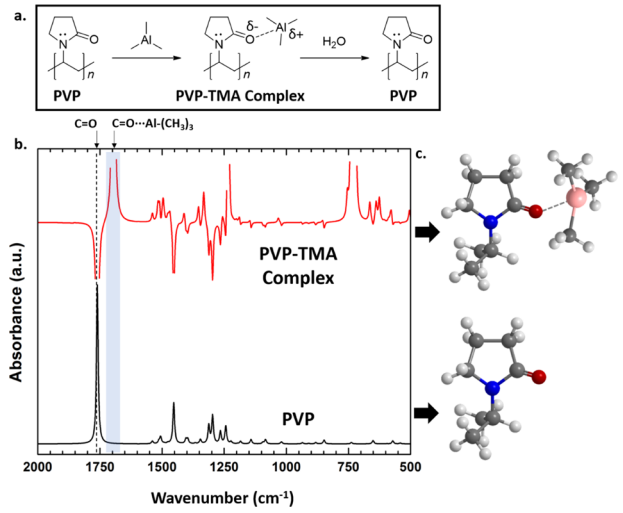

Figure 4. (a) Proposed sequence of PVP−TMA complex formation and removal. (b) Computed vibrational spectra referenced to spectra calculated from PVP structures in the absence of TMA. (c) Relaxed chemical structures calculated using ab initio analysis.

calculations are shown for the corresponding species to the right (Figure 4c). In the spectra, the dotted line at 1760 cm^{-1} corresponds to C═O stretching, which switches from a positive-going mode for PVP to a negative-going mode for the PVP−TMA complex. The complex also exhibits a positive-going mode at 1696 cm^{-1}, which corresponds to the C═O···Al−$(CH_3)_3$ Lewis acid/base adduct. These calculated spectra replicate the spectra changes in the experimental results, thus verifying the proposed mechanism.

Poly(acrylic acid). Another functional group of interest with structural similarity to PMMA is the carboxylic acid in PAA. The key difference between the two is the acidic hydrogen bonded to the oxygen in PAA in contrast to the methyl group bonded to the oxygen in PMMA. Figure 5 shows the spectra of PAA upon dosing at 60, 100, and 150 °C. The characteristic modes of PAA are seen at 1712, 1448, and 1280 cm^{-1}, which are the C═O stretching, C−H bending (δ(C−H)), and C−O stretching modes, respectively. PAA contains a

DOI: 10.1021/acs.jpcc.9b02153
J. Phys. Chem. C 2019, 123, 16146−16152

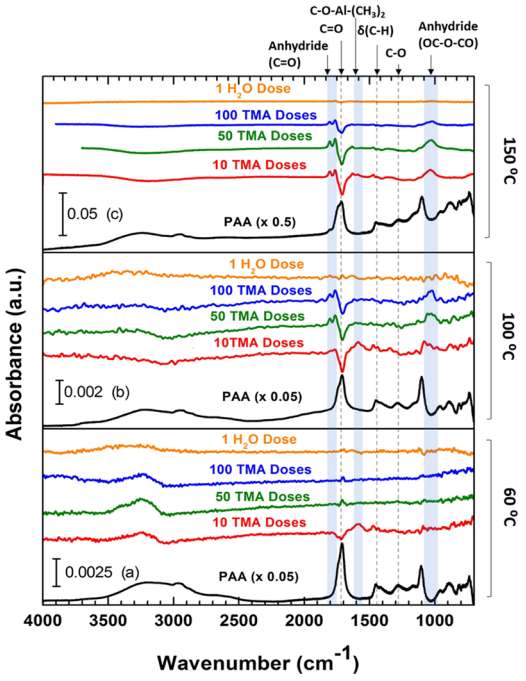

Figure 5. In situ FTIR spectra taken after n TMA doses at (a) 60 °C, (b) 100 °C, and (c) 150 °C on PAA film. The black spectrum is the PAA referenced to the bare silicon substrate, and all other spectra are referenced to the previous spectrum.

carboxylic acid moiety, and TMA is known to react readily with hydroxyl surfaces.[33] From this information, it was hypothesized that TMA would readily form a covalent bond with PAA. In Figure 5a, after 10 TMA doses at 60 °C, there is a negative-going mode at 1712 cm^{-1} and a positive-going mode at 1585 cm^{-1}. These modes are consistent with a shift from the original C═O stretching to a new C═O stretching accompanied by C−O−Al−$(CH_3)_2$, the new TMA−PAA covalent bond. There is also a positive-going mode at 1448 cm^{-1}, which corresponds to the increase of C−H groups from the TMA addition. The largest change happens after the first 10 TMA doses, and the following changes after each TMA dosing cycle are much smaller.

After the water dose, the differential spectrum remains the same. We infer that the C═O reacted with TMA to form a covalent bond. The availability of the acidic proton allows for the covalent metal−organic bonds to form readily. Without the acidic proton, the covalent metal−organic bond depends on the stability of the metastable TMA−carbonyl group complex. The absence of a sufficiently reactive functional group may also be the reason for the presence of Al−O in PMMA and PVP, indicated by positive-going modes at 820 cm^{-1} in the respective spectra.

After the first 10 TMA doses at 100 °C on PAA, shown in Figure 5b, the same negative-going mode at 1712 cm^{-1} and positive-going mode at 1585 cm^{-1} seen at 60 °C are present. The modes appear with a greater intensity at an elevated temperature. After an additional 40 TMA doses, there is a continued decrease of the carbonyl stretching mode at 1712 cm^{-1}. There is a new formation of a doublet with positive-going modes at 1805 and 1762 cm^{-1}, which is consistent with the C═O stretching of an anhydride. The new positive-going mode at 1030 cm^{-1} is consistent with the OC−O−CO stretching of an anhydride. Therefore, this new doublet and positive-going mode suggest the formation of an anhydride functionality. The anhydride formation continued after another 50 TMA doses. After the water dose, the differential water spectrum is constant; thus, the anhydride structures remain present. From the TMA doses on PAA at 150 °C, shown in Figure 5c, the anhydride forms after the first 10 TMA doses and at a higher intensity (at 1805, 1762, and 1030 cm^{-1}). The anhydride formation continues through the following TMA doses and remains the same after the water dose. This indicates that the new formations are stable, covalent modifications. It is well known that PAA can form anhydride functional groups thermally, which typically occurs once temperatures are greater than 200 °C.[34] Since anhydrides are forming at lower temperatures, we infer that Lewis acid-catalyzed anhydride synthesis is occurring. Cyclic anhydrides are reactive to nucleophiles, which could extend the polymer side chains with the addition of new reactants and introduce the ability to develop more complex hybrid materials.

From the analysis of the experimental spectra in Figure 5, we conclude that PAA and TMA go through a pericyclic reaction, shown in Figure 6a, to form the PAA−aluminum acetate and

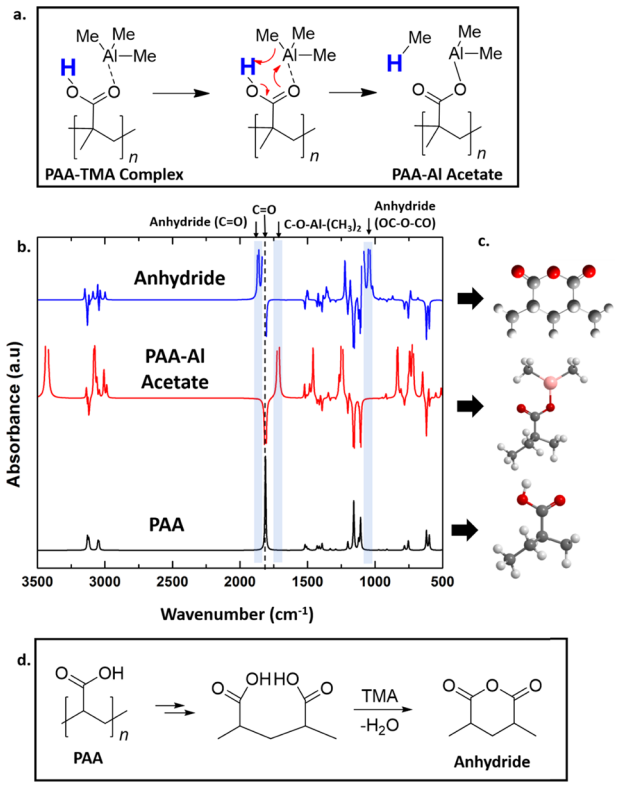

Figure 6. (a) Proposed pericyclic reaction of carboxylic acid to form metal acetate. (b) Computed vibrational spectra referenced to spectra calculated from PMMA structures in the absence of TMA. (c) Relaxed chemical structures calculated using ab initio analysis. (d) Proposed sequence of anhydride formation.

methane. This reaction is comparable to the PMMA−TMA reaction mechanism, which produces PMMA−aluminum acetate and ethane. The key difference is that the PAA−TMA reaction occurs at $T \leq 100$ °C and the PMMA−TMA reaction occurs at higher temperatures. The reactivity of the acidic hydrogen in the PAA likely lowers the activation energy of the proposed pericyclic reaction mechanism, thus allowing

DOI: 10.1021/acs.jpcc.9b02153
J. Phys. Chem. C 2019, 123, 16146−16152

the reaction to proceed at a lower temperature in PAA than in PMMA.

The spectra from frequency calculations of PAA−aluminum acetate product and PAA are shown in Figure 6b. The molecule structures used for modeling the PAA−aluminum acetate and PAA are shown in Figure 6c. The characteristic C═O stretch is shown as a positive-going mode at 1813 cm^{-1}. The PAA−aluminum acetate has a negative-going mode at 1813 cm^{-1} and a positive-going mode at 1709 cm^{-1}, which corresponds to the shift in the C═O stretch vibration and upon formation of C−O−Al$(CH_3)_2$ bonding. There is also a positive-going mode at 1459 cm^{-1}, which corresponds to an increase in the C−H bending (δ(C−H)) from the TMA. These modes correspond to those seen in the experimental data, thus backing the reaction mechanism proposed in Figure 6a. The anhydride formation hypothesized at higher temperatures was also investigated computationally. The proposed reaction mechanism for Lewis acid-catalyzed anhydride synthesis scheme is shown in Figure 6d. The computed frequencies for the anhydride are shown in the top spectrum of Figure 6b, and the computed structure is shown in the top model in Figure 6c. The doublet positive-going modes at 1837 and 1871 cm^{-1} and the positive-going mode at 1037 cm^{-1} correspond to the modes attributed to anhydride formation in the experimental data. This anhydride formation results in a loss of water from the system.

CONCLUSIONS

The collective findings from the in situ FTIR and the ab initio quantum chemical analysis support the conclusion that chemical functionality is a critical factor in predicting the chemical interactions from infusing TMA vapor into polymer thin films via the SVI process. We find that when dosing carbonyl-containing polymers with a strong Lewis acid like TMA, the precursor tends to begin by forming a metastable C═O···Al−$(CH_3)_3$ complex. Unless a subsequent reaction forms a covalent bond between the precursor and the substrate, this complex will break apart during the SVI water dose. The complex can go on to bond itself to the substrate through a concerted, pericyclic reaction mechanism that forms an Al−O bond, resulting in a C−O−Al−$(CH_3)_2$ group. The activation energy of this pericyclic reaction mechanism is highly dependent on the functional groups neighboring the carbonyl. In PVP, the activation energy of this reaction is likely too high for the reaction to occur until temperatures higher than those measured in this study. In PMMA, the activation energy is lower than in PVP, but still high enough that the reaction was not seen until 150 °C. In PAA, the acidic proton of the carboxylic acid lowers the activation energy of this reaction enough that the reaction occurs at temperatures as low as 60 °C. The presence of the acidic proton in PAA also allows a second reaction mechanism to occur, forming a cyclic anhydride group that, with the addition of a nucleophile, could be a powerful tool for creating, extending, and modifying polymer side chains. The variation in the activation energy of the pericyclic reaction mechanism between the three polymers and the presence of a second reaction mechanism in PAA highlight the potential that different polymer pendant groups have to change the behavior and utility of the SVI process. Small changes in the substituent function groups of a polymer can lead to large gains in substrate−precursor reactivity and even create opportunities for polymer chain modification and functionalization that were previously not present. This understanding of the role that chemical functional groups play during SVI processes with TMA will help assist the future rapid synthesis of hybrid materials for various applications.

AUTHOR INFORMATION

Corresponding Author

*E-mail: gnp@ncsu.edu.

ORCID

Grant T. Hill: 0000-0002-6344-304X

Dennis T. Lee: 0000-0002-1976-2852

Gregory N. Parsons: 0000-0002-0048-5859

Author Contributions

The manuscript was written through contributions of all authors. All authors have given approval to the final version of the manuscript.

Notes

The authors declare no competing financial interest.

ACKNOWLEDGMENTS

The authors acknowledge funding from the US National Science Foundation, Award No. 1704151.

ABBREVIATIONS

SVI, sequential vapor infiltration; PMMA, poly(methyl methacrylate); PVP, poly(vinylpyrrolidone); PAA, poly(acrylic acid); VPI, vapor-phase infiltration; ALD, atomic layer deposition; MOFs, metal−organic frameworks; FTIR, Fourier transform infrared spectroscopy

REFERENCES

(1) Leng, C. Z.; Losego, M. D. Vapor phase infiltration (VPI) for transforming polymers into organic−inorganic hybrid materials: a critical review of current progress and future challenges. *Mater. Horiz.* **2017**, *4*, 747−771.

(2) Dandley, E. C.; Needham, C. D.; Williams, P. S.; Brozena, A. H.; Oldham, C. J.; Parsons, G. N. Temperature-dependent reaction between trimethylaluminum and poly(methyl methacrylate) during sequential vapor infiltration: experimental and ab initio analysis. *J. Mater. Chem. C* **2014**, *2*, 9416−9424.

(3) Padbury, R. P.; Jur, J. S. Temperature-dependent infiltration of polymers during sequential exposures to trimethylaluminum. *Langmuir* **2014**, *30*, 9228−9238.

(4) Akyildiz, H. I.; Padbury, R. P.; Parsons, G. N.; Jur, J. S. Temperature and exposure dependence of hybrid organic − inorganic layer formation by sequential vapor infiltration into polymer fibers. *Langmuir* **2012**, *28*, 15697−15704.

(5) Zhao, J.; Losego, M. D.; Lemaire, P. C.; Williams, P. S.; Gong, B.; Atanasov, S. E.; Blevins, T. M.; Oldham, C. J.; Walls, H. J.; Shepherd, S. D.; et al. Highly adsorptive, MOF-functionalized nonwoven fiber mats for hazardous gas capture enabled by atomic layer deposition. *Adv. Mater. Interfaces* **2014**, *1*, No. 1400040.

(6) Zhao, J.; Gong, B.; Nunn, W. T.; Lemaire, P. C.; Stevens, E. C.; Sidi, F. I.; Williams, P. S.; Oldham, C. J.; Walls, H. J.; Shepherd, S. D.; et al. Conformal and highly adsorptive metal-organic framework thin films via layer-by-layer growth on ALD-coated fiber mats. *J. Mater. Chem. A* **2015**, *3*, 1458−1464.

(7) Zhao, J.; Nunn, W. T.; Lemaire, P. C.; Lin, Y.; Dickey, M. D.; Oldham, C. J.; Walls, H. J.; Peterson, G. W.; Losego, M. D.; Parsons, G. N. Facile conversion of hydroxy double salts to metal−organic frameworks using metal oxide particles and atomic layer deposition thin-film templates. *J. Am. Chem. Soc.* **2015**, *137*, 13756−13759.

(8) Zhao, J.; Lee, D. T.; Yaga, R. W.; Hall, M. G.; Barton, H. F.; Woodward, I. R.; Oldham, C. J.; Walls, H. J.; Peterson, G. W.; Parsons, G. N. Ultra-fast degradation of chemical warfare agents using

DOI: 10.1021/acs.jpcc.9b02153
J. Phys. Chem. C 2019, 123, 16146−16152

MOF-nanofiber kebabs. *Angew. Chem., Int. Ed.* **2016**, *55*, 13224−13228.
(9) Lee, D. T.; Zhao, J.; Peterson, G. W.; Parsons, G. N. Catalytic "MOF-cloth" formed via directed supramolecular assembly of UiO-66-NH2 crystals on atomic layer deposition-coated textiles for rapid degradation of chemical warfare agent simulants. *Chem. Mater.* **2017**, *29*, 4894−4903.
(10) Lee, D. T.; Zhao, J.; Oldham, C. J.; Peterson, G. W.; Parsons, G. N. UiO-66-NH2 MOF nucleation on TiO_2, ZnO, and Al_2O_3 ALD-treated polymer fibers: role of metal oxide on MOF growth and catalytic hydrolysis of chemical warfare agent simulants. *ACS Appl. Mater. Interfaces* **2017**, *9*, 44847−44855.
(11) Lee, S.; Pippel, E.; Gösele, U.; Dresbach, C.; Qin, Y.; Chandran, C. V.; Bräuniger, T.; Hause, G.; Knez, M. Greatly increased toughness of infiltrated spider silk. *Science* **2009**, *324*, 488−492.
(12) Lee, S. M.; Pippel, E.; Moutanabbir, O.; Gunkel, I.; Thurn-Albrecht, T.; Knez, M. Improved mechanical stability of dried collagen membrane after metal infiltration. *ACS Appl. Mater. Interfaces* **2010**, *2*, 2436−2441.
(13) Dandley, E. C.; Lemaire, P. C.; Zhu, Z.; Yoon, A.; Sheet, L.; Parsons, G. N. Correction to: wafer-scale selective-area deposition of nanoscale metal oxide features using vapor saturation into patterned poly(methyl methacrylate) templates. *Adv. Mater. Interfaces* **2017**, *4*, 1−9.
(14) Tseng, Y. C.; Peng, Q.; Ocola, L. E.; Elam, J. W.; Darling, S. B. Enhanced block copolymer lithography using sequential infiltration synthesis. *J. Phys. Chem. C* **2011**, *115*, 17725−17729.
(15) Ishchenko, O. M.; Krishnamoorthy, S.; Valle, N.; Guillot, J.; Turek, P.; Fechete, I.; Lenoble, D. Investigating sequential vapor infiltration synthesis on block-copolymer-templated titania nano-arrays. *J. Phys. Chem. C* **2016**, *120*, 7067−7076.
(16) Segal-Peretz, T.; Winterstein, J.; Doxastakis, M.; Ramírez-Hernández, A.; Biswas, M.; Ren, J.; Suh, H. S.; Darling, S. B.; Liddle, J. A.; Elam, J. W.; et al. Characterizing the three-dimensional structure of block copolymers via sequential infiltration synthesis and scanning transmission electron tomography. *ACS Nano* **2015**, *9*, 5333−5347.
(17) Obuchovsky, S.; Deckman, I.; Moshonov, M.; Segal Peretz, T.; Ankonina, G.; Savenije, T. J.; Frey, G. L. Atomic layer deposition of zinc oxide onto and into P3HT for hybrid photovoltaics. *J. Mater. Chem. C* **2014**, *2*, 8903−8910.
(18) Gong, B.; Spagnola, J. C.; Parsons, G. N. Hydrophilic mechanical buffer layers and stable hydrophilic finishes on polydimethylsiloxane using combined sequential vapor infiltration and atomic/molecular layer deposition. *J. Vac. Sci. Technol., A* **2012**, *30*, No. 01A156.
(19) Gong, B.; Peng, Q.; Jur, J. S.; Devine, C. K.; Lee, K.; Parsons, G. N. Sequential vapor infiltration of metal oxides into sacrificial polyester fibers: shape replication and controlled porosity of microporous/mesoporous oxide monoliths. *Chem. Mater.* **2011**, *23*, 3476−3485.
(20) Gong, B.; Kim, D.; Parsons, G. N. Mesoporous metal oxides by vapor infiltration and atomic layer deposition on ordered surfactant polymer films. *Langmuir* **2012**, *28*, 11906−11913.
(21) Wilson, C. A.; Grubbs, R. K.; George, S. M. Nucleation and growth during Al_2O_3 atomic layer deposition on polymers. *Chem. Mater.* **2005**, *17*, 5625−5634.
(22) Hyde, G. K.; Park, K. J.; Stewart, S. M.; Hinestroza, J. P.; Parsons, G. N. Atomic layer deposition of conformal inorganic nanoscale coatings on three-dimensional natural fiber systems: effect of surface topology on film growth characteristics. *Langmuir* **2007**, *23*, 9844−9849.
(23) Biswas, M.; Libera, J. A.; Darling, S. B.; Elam, J. W. New insight into the mechanism of sequential infiltration synthesis from infrared spectroscopy. *Chem. Mater.* **2014**, *26*, 6135−6141.
(24) Biswas, M.; Libera, J. A.; Darling, S. B.; Elam, J. W. Kinetics for the sequential infiltration synthesis of alumina in poly(methyl methacrylate): an infrared spectroscopic study. *J. Phys. Chem. C* **2015**, *119*, 14585−14592.
(25) Parsons, G. N.; Atanasov, S. E.; Dandley, E. C.; Devine, C. K.; Gong, B.; Jur, J. S.; Lee, K.; Oldham, C. J.; Peng, Q.; Spagnola, J. C.; et al. Mechanisms and reactions during atomic layer deposition on polymers. *Coord. Chem. Rev.* **2013**, *257*, 3323−3331.
(26) Suzuki, T.; Saimoto, H.; Tomioka, H.; Oshima, K.; Nozaki, H. Regio- and stereoselective ring opening of epoxy alcohols with organoaluminium compounds leading to 1,2-diols. *Tetrahedron Lett.* **1982**, *23*, 3597−3600.
(27) Jur, J. S.; Spagnola, J. C.; Lee, K.; Gong, B.; Peng, Q.; Parsons, G. N. Temperature-dependent subsurface growth during atomic layer deposition on polypropylene and cellulose fibers. *Langmuir* **2010**, *26*, 8239−8244.
(28) Frisch, M. J.; Trucks, G. W.; Schlegel, H. B.; Scuseria, G. E.; Robb, M. A.; Cheeseman, J. R.; Scalmani, G.; Barone, V.; Mennucci, B.; Petersson, G. A.; et al. *Gaussian 09*, revision D.01; Gaussian Inc.: Wallingford, CT, 2009.
(29) Wong, M. W. Vibrational frequency prediction using density functional theory. *Chem. Phys. Lett.* **1996**, *256*, 391−399.
(30) Scott, A. P.; Radom, L. Harmonic Vibrational Frequencies: An evaluation of Hartree−Fock, Møller−Plesset, quadratic configuration interaction, density functional theory, and semiempirical scale factors. *J. Phys. Chem. A* **1996**, *100*, 16502−16513.
(31) Dennington, R.; Keith, T.; Millam, J. *GaussView*; Semichem Inc.: Shawnee Mission, KS, 2009.
(32) Takai, K.; Mori, I.; Oshima, K.; Noazki, H. Aliphatic Claisen rearrangement promoted by organoaluminium reagents. *Bull. Chem. Soc. Jpn.* **1984**, *57*, 446−451.
(33) Xu, Y.; Musgrave, C. B. A DFT study of the Al_2O_3 atomic layer deposition on SAMs: effect of SAM termination. *Chem. Mater.* **2004**, *16*, 646−653.
(34) Mcneill, I. C.; Sadeghi, S. M. T. Thermal stability and degradation mechanisms of poly(acrylic acid) and its salts. Part 1. Poly(acrylic acid). *Polym. Degrad. Stab.* **1990**, *29*, 233−246.

DOI: 10.1021/acs.jpcc.9b02153
J. Phys. Chem. C 2019, 123, 16146−16152